

Open Research Online

The Open University's repository of research publications and other research outputs

Analysing the consistency of martian methane observations by investigation of global methane transport

Journal Item

How to cite:

Holmes, James A.; Lewis, Stephen R. and Patel, Manish R. (2015). Analysing the consistency of martian methane observations by investigation of global methane transport. *Icarus*, 257 pp. 23–32.

For guidance on citations see [FAQs](#).

© 2015 The Authors



<https://creativecommons.org/licenses/by/4.0/>

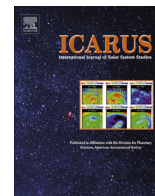
Version: Version of Record

Link(s) to article on publisher's website:

<http://dx.doi.org/doi:10.1016/j.icarus.2015.04.027>

Copyright and Moral Rights for the articles on this site are retained by the individual authors and/or other copyright owners. For more information on Open Research Online's data [policy](#) on reuse of materials please consult the policies page.

oro.open.ac.uk



Analysing the consistency of martian methane observations by investigation of global methane transport



James A. Holmes^{a,*}, Stephen R. Lewis^a, Manish R. Patel^{a,b}

^a Department of Physical Sciences, The Open University, Milton Keynes MK7 6AA, UK

^b Space Science and Technology Department, STFC Rutherford Appleton Laboratory, Chilton, Didcot, Oxfordshire OX11 0QX, UK

ARTICLE INFO

Article history:

Received 29 September 2014

Revised 15 April 2015

Accepted 15 April 2015

Available online 20 April 2015

Keywords:

Mars, atmosphere

Atmospheres, evolution

Meteorology

ABSTRACT

Reports of methane on Mars at different times imply varying spatial distributions. This study examines whether different observations are mutually consistent by using a global circulation model to investigate the time evolution of methane in the atmosphere. Starting from an observed plume of methane, consistent with that reported in 2003 from ground-based telescopes, multiple simulations are analysed to investigate what is required for consistency with an inferred methane signal from the Thermal Emission Spectrometer made 60 sols later.

The best agreement between the existing observations is found using continued release from a solitary source over Nili Fossae. While the peaks in methane over the Tharsis Montes, Elysium Mons and Nili Fossae regions are well aligned with the retrievals, an extra peak on the south flank of the Isidis basin is apparent in the model due to the prevailing eastward transport of methane. The absence of this feature could indicate the presence of a fast-acting localised sink of methane.

These results show that the spatial and temporal variability of methane on Mars implied by observations could be explained by advection from localised time-dependent sources alongside a currently unknown methane sink. Evidence is presented that a fast trapping mechanism for methane is required. Trapping by a zeolite structure in dust particles is a suggested candidate warranting further investigation; this could provide a fast acting sink as required by this reconstruction.

© 2015 The Authors. Published by Elsevier Inc. This is an open access article under the CC BY license (<http://creativecommons.org/licenses/by/4.0/>).

1. Introduction

Observations of methane on Mars have come from both ground-based telescopes (Krasnopolsky et al., 2004; Mumma et al., 2009) and orbiters (Formisano et al., 2004; Fonti and Marzo, 2010) with maximum values ranging from 10 to 60 ppb. More recently, the NASA Curiosity rover has measured a sudden increase in methane in Gale crater to 7 ppb (Webster et al., 2015) after previously providing an *in situ* local upper limit of 1.3 ppb (Webster et al., 2013). The possibility of methane as a biomarker for extraterrestrial life means its existence is significant, although geological origin cannot be ruled out either (Atreya et al., 2007). The reported observations from multiple instruments vary in methane abundance and spatial distribution, with no general agreement. Suggested processes to create methane in the atmosphere range from volcanic hotspots and serpentinization to cometary impacts and microorganisms with some of these sources more feasible than others (Atreya et al., 2007). The origin of source(s) of methane will not be addressed in this investigation.

The long lifetime of methane (300 years) implies it should become well mixed in the atmosphere (Lefèvre and Forget, 2009). Additional destruction mechanisms are required to explain the apparent variability observed. With a much shorter lifetime in the atmosphere of 200 days, Lefèvre and Forget (2009) demonstrate the local enhancements of methane observed could be potentially reconstructed. Destruction mechanisms theorised include electrochemical processes during dust storms (Farrell et al., 2006), a reactive surface due to a strong oxidiser such as H₂O₂ (Atreya et al., 2006) and loss to the regolith (Gough et al., 2010). Lefèvre and Forget (2009) dismiss electrochemical processes due to the extreme bulk electric field needed and their effect on other chemical species which are well simulated without these added processes. Strong oxidation by H₂O₂ was investigated by Gough et al. (2011) with the conclusion that a very deep soil layer greater than 500 m in depth is required for rapid loss of methane from the atmosphere. Loss to the regolith was also determined to be too slow by Meslin et al. (2011). Surface loss of methane is reliant on the composition and structure of the martian regolith and the uptake coefficient of the surface.

Mischna et al. (2011) investigated the creation of the plume identified by Mumma et al. (2009), concluding that their best fit

* Corresponding author.

E-mail address: james.holmes@open.ac.uk (J.A. Holmes).

source indicated the plume of methane would have needed to form in 1–2 sols. In their study, the potential of computer models in constraining the source of tracer plumes is clearly evident. Exploring the consistency of past observations of methane measured by different instruments and at different points in time using source/sink experiments is yet to be undertaken.

In this study a global circulation model (GCM) is used to investigate the consistency of past methane measurements by analysing the transport of methane from source emission. The next section describes the initial setup of the GCM. The simulations for the investigation are detailed followed by results on the tracer transport diagnostics from the simulations. A comparison of the simulations and possible destruction mechanisms are then discussed. The significance of this study regarding the NASA Curiosity rover results is then described.

2. Method

This investigation uses the UK version of the LMD GCM which has been developed in a collaboration of the Laboratoire de Météorologie Dynamique, the Open University, the University of Oxford and the Instituto de Astrofísica de Andalucía. This model uses physical parameterisations (Forget et al., 1999) shared with the LMD GCM. These are coupled to a spectral dynamical core and semi-lagrangian advection scheme (Newman et al., 2002) to transport tracers.

The dust distribution has been prescribed horizontally using an interpolation of numerous sets of observations from orbiters and landers using a kriging method (Montabone et al., 2015) and vertically using the Conrath dust profile. The model was truncated at wavenumber 31 resulting in a 5° longitude–latitude grid with 32 vertical levels extending to an altitude of ~ 100 km.

Methane is transported using a semi-lagrangian advection scheme with mass conservation (Priestley, 1993). The advection scheme uses wind fields updated by the dynamical core to determine the methane concentration at each model grid point every 30 min. For the best possible representation of atmospheric state, temperature retrievals from the Thermal Emission Spectrometer (TES) are assimilated (Lewis et al., 2007). The model ensures the wind field is consistent with thermal data. This provides the best constraint available on the transport of methane in the atmosphere since there are no direct wind observations. Lewis et al. (2007) also showed that actual transient wave behaviour seen in observations is captured by the model when assimilating TES temperature profiles, rather than simply modifying the thermal state of the model to produce transient modes of different strengths and locations.

For all simulations in this paper the initial column-average methane mixing ratio is as shown in Fig. 1 in an effort to closely match the observations in 2003 ($L_S = 122$ – 155° Mars year [MY] 26) by Mumma et al. (2009). The observations cover only half the surface. A simulation which included zero methane across all latitudes from 180°E to 0° resulted in the same spatial distribution as a simulation initialised as shown in Fig. 1 with slightly lower levels in methane abundance. This suggests minimal sensitivity of the simulation to the initial distribution of column-average methane mixing ratio in this unobserved region.

Since column-averaged mixing ratios have been retrieved with no information on the vertical structure, the initial mass mixing ratio of methane was spread in the vertical using the weighting function

$$f(\sigma) = \begin{cases} \frac{1}{2} + \frac{1}{2} \cos\left(\frac{-10\pi \ln(\sigma)}{z_{\max}}\right), & \text{if } z \leq z_{\max} \\ 0, & \text{otherwise} \end{cases}$$

where $\sigma = p/p_s$ is the sigma level of the model (atmospheric pressure p scaled by the surface pressure p_s) and z_{\max} is the maximum

altitude for methane to still be present initially in the atmospheric column. For the simulations, the maximum initial altitude of methane was set at 10 km. Tests using 30 km and 50 km for z_{\max} showed little difference, in agreement with Mischna et al. (2011). No initial assumption about whether the observations were retrieved at the start, middle or end of the methane release is made. Continued emission from the localised sources identified by Mumma et al. (2009) is entirely plausible.

3. Simulations

To investigate the transport of methane by different surface sources, four simulations are run as displayed in Table 1. The control run includes no additional sources or sinks of methane. The MuS run includes a source identified by Mumma et al. (2009) over Nili Fossae. The MiS run includes the best fit source emission from Mischna et al. (2011) which is much more extensive in latitude than the other simulations. The TS run is similar to the MuS run but includes an additional source over the Tharsis region, where initially methane was unobserved by Mumma et al. (2009).

The rate of emission in Table 1 has been calculated to closely match the maximum methane abundance inferred by Fonti and Marzo (2010) at $L_S = 180^\circ$ MY 26 (hereafter FM10 signal). No additional constraint on where the maximum methane abundance is located spatially on the globe for each simulation is made. Source emission of any strength for the whole period in between the observations resulted in the source still evident in the distribution at $L_S = 180^\circ$. Therefore, a continued source emission must have stopped within ~ 50 sols of the original plume to allow time for dispersion of methane over the source location. For ease of analysis, the source emission occurs for the first 30 sol period ($L_S = 148$ – 164°) of each simulation (except the control run which has no source). Where methane is being emitted by a surface source, the methane mass mixing ratio q in the lowest level in the atmosphere is given an additional increase after each timestep of $q = q + (\Phi_m g \Delta t) / \Delta p$ where Φ_m is the source surface flux ($\text{kg m}^{-2} \text{s}^{-1}$), Δt is the timestep (s) and Δp is the pressure difference between the lowest two levels of the atmosphere (Pa). This extra emission adds to the local methane mass and, along with the methane already present in the atmosphere, is advected by the transport scheme each timestep.

To match the maximum methane abundance in the FM10 signal, the MuS simulation required a single source strength of $\Phi_m = 10^{-9} \text{ kg m}^{-2} \text{s}^{-1}$ over the $5^\circ \times 5^\circ$ grid box, resulting in 85 kg of methane added to the atmosphere every second. The formation of the observed initial plume by Mumma et al. (2009) was investigated by Mischna et al. (2011) with their best fit conclusion being a rapid build up of the plume over 1–2 sols before the observations. To create the initial plume mass of $1.86 \times 10^7 \text{ kg}$ over 2 sols would require over 100 kg of methane to be added to the atmosphere each second. Also, a recent investigation by Stevens et al. (2015) regarding the transport of methane in the martian subsurface indicate gas released by the destabilisation of methane clathrate hydrates close to the surface could potentially provide a flux of as much as $10^{-3} \text{ kg m}^{-2} \text{s}^{-1}$ over a duration of less than half an MY.

4. Atmospheric transport of methane: A case study

This section describes the advection of methane in the four different simulations identified above in Table 1. The simulations were all initialised with the exact same methane distribution (Fig. 1) and all simulations, with the exception of the control run, include a surface source of methane for the first 30 sols ($L_S = 148$ – 164° MY 26). In the following 30 sols ($L_S = 164$ – 181° MY 26), methane is simply advected in each simulation by

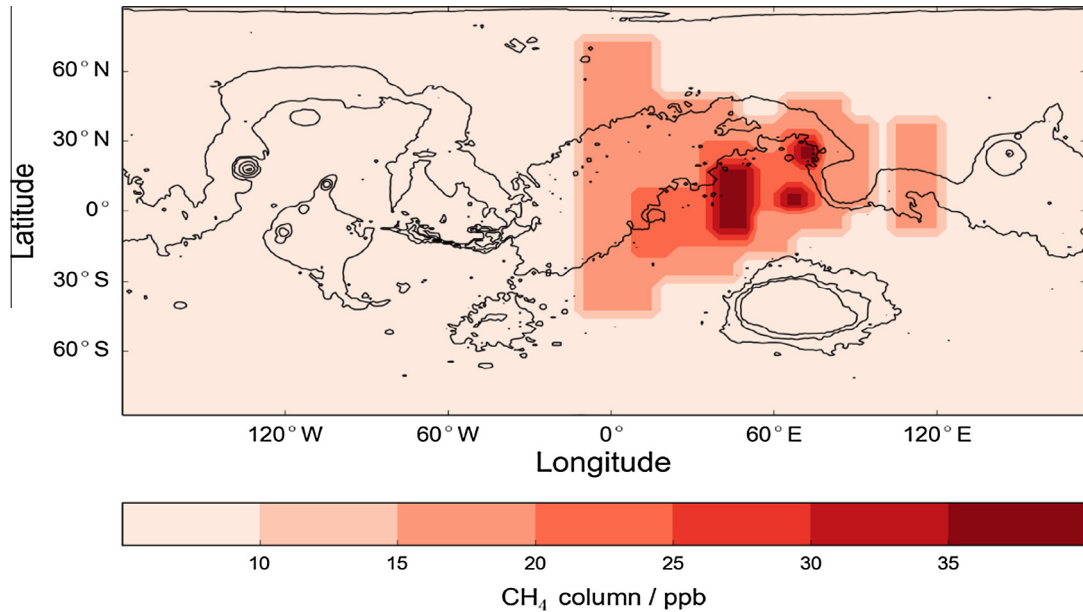


Fig. 1. Column-average methane mixing ratio at the start of the GCM simulation. The simulations begin at $L_S = 148^\circ$ since the identified peaks in volume-average methane mixing ratio were measured by Mumma et al. (2009) towards the end of their observation period in 2003 ($L_S = 122\text{--}155^\circ$).

Table 1

Details of the different simulations run over the 60 sol period investigated.

Simulation	Emission from $L_S = 148\text{--}164^\circ$	Rate of emission [Φ_m] ($\text{kg m}^{-2} \text{s}^{-1}$)
Control	None	–
MuS	Surface emission at 2.5°N , 50°E	10^{-9}
MiS	Surface emission in a parallelogram covering $30\text{--}70^\circ\text{E}$ and $37.5^\circ\text{S}\text{--}37.5^\circ\text{N}$	3.0×10^{-11}
TS	Surface emission at 2.5°N , 50°E and 2.5°N , 90°W	0.5×10^{-9}

transport processes with no further source emission. Since the presence of methane does not affect the heating of the atmosphere, the wind field is the same for all four simulations.

The zonal and meridional transport of methane is decomposed into three separate constituents following Peixoto and Oort (1992) as

$$[\overline{qa}] = [\overline{q}][\overline{a}] + [\overline{q'}a'] + [\overline{q'a'}], \quad \text{for } a = u, v$$

where u and v are the zonal and meridional wind respectively, the overbar represents a time-average and the square brackets represent a zonal-average. Through this decomposition, the magnitude of transport due to the mean circulation ($[\overline{q}][\overline{a}]$), stationary eddies ($[\overline{q'}a']$) and transient eddies ($[\overline{q'a'}]$) can be compared. Deviations of the variable from the time and zonal mean are represented by the prime and star symbol respectively. Hinson (2006) found transient eddies to at most have a period of 10 sols on Mars, therefore a 30 sol time average is sufficient to sample multiple eddies. Results on the transport of methane in this case study are split into the two previously mentioned 30 sol periods to distinguish between the time period in which source emission occurs and after emission has ceased.

4.1. $L_S = 148\text{--}164^\circ$: Source release

The vertically integrated zonal and meridional flux on each latitude circle for the control run are displayed in Fig. 2a and b respectively. Over this time period, the southern jet is beginning to

weaken after peak southern winter conditions and the northern jet is beginning to form as autumnal equinox approaches.

The primary transport of methane zonally is eastward for all simulations and is dominated by the mean circulation component. The mean circulation of meridional flux (Fig. 2b) transports mid-latitude methane towards the equator due to two roughly symmetrical Hadley cells which both have a rising branch centred near to the equator at this time of year. Transport by stationary and transient eddies generally opposes the mean circulation resulting in little overall transport of methane meridionally. Changes in the zonal and meridional flux of methane from the control run are attributed to changes in the local mass mixing ratio of methane since the wind field is the same for all simulations.

With the source in the MuS run emitting for the 30 sol period, the overall zonal transport is increased in both hemispheres. The zonal transport just above the equator has increased considerably to form an almost symmetrical pattern around the equator (Fig. 2c). The large increase in mass of methane at the source location, coupled with weak surface winds, provides the peak in zonal transport at 2.5°N . A stationary eddy south of Nili Fossae (Fig. 3a), coupled to the mean circulation directly below the source location (Fig. 3c), decrease the net eastward transport of methane just south of the equator. This activity immediately below the source location causes the elevated levels of methane to expand along a SW–NE line centred on the source location. Fig. 3c also indicates that methane is primarily transported eastward away from the source in the mid-latitude regions of the north and south hemisphere over Nili Fossae and Hellas basin respectively.

Two peaks in transport north and south of the equator are also noticeable in the meridional flux (Fig. 2d). This feature is due to transient eddies, which account for $\sim 65\%$ of the meridional transport close to the equator. The identified peaks are almost entirely due to the surface source emission, as evident in Fig. 3d, with the meridional transport an order of magnitude larger than in the control run (Fig. 2b). The continuous release of methane over time provides peak transport directly north and south of the source by weak surface meridional winds coupled to the increased mass of methane.

The broad source in the MiS run acts primarily to enhance the control run zonal flux profile, with an increase in zonal methane flux

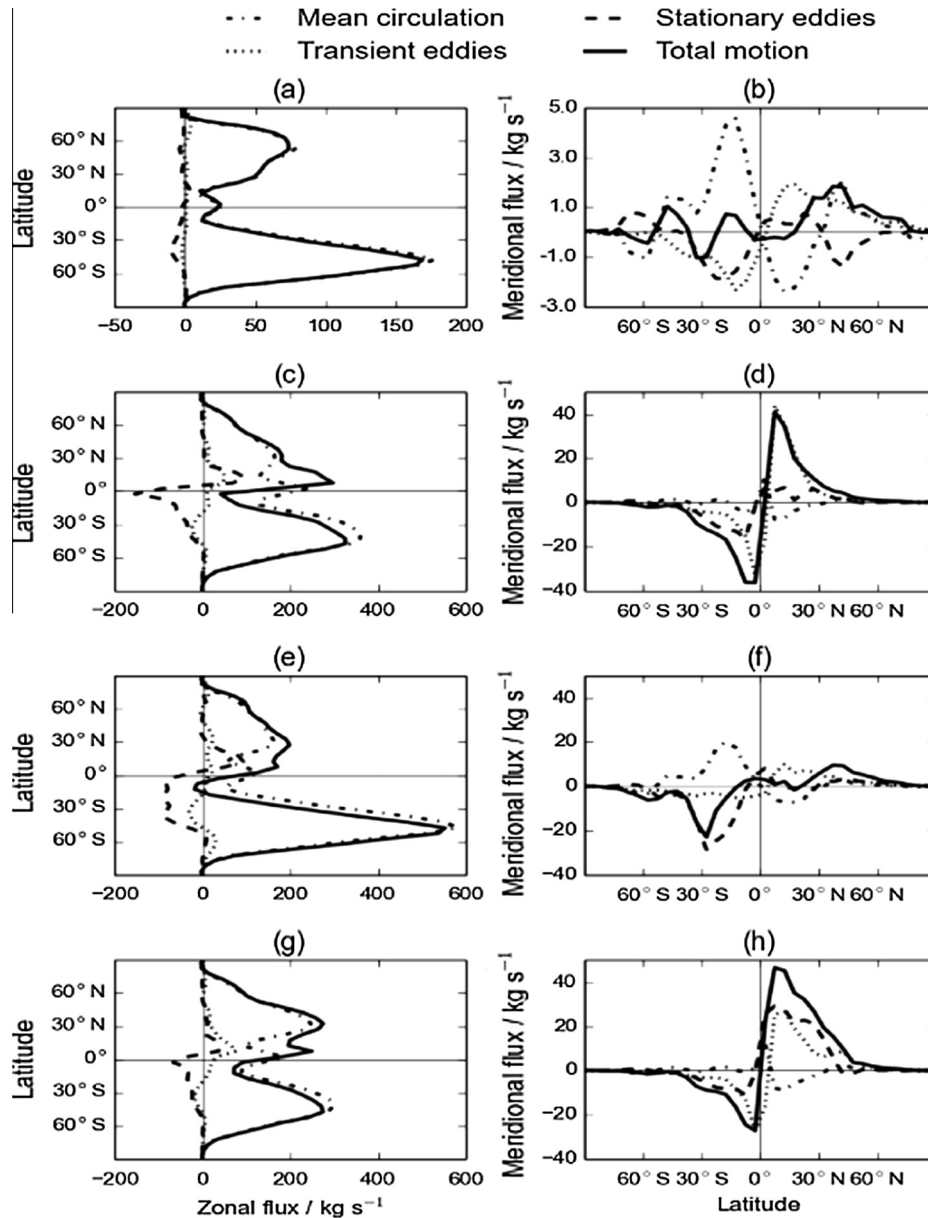


Fig. 2. Vertically integrated zonal (left) and meridional (right) flux of methane for each latitude band in the control (a and b), MuS (c and d), MiS (e and f) and TS (g and h) runs from $L_S = 148$ – 164° MY 26. Note the change of scale for zonal and meridional flux in (a) and (b). Eastward and northward flux are positive.

of around 3 for most latitude bands peaking at 540 kg s^{-1} (Fig. 2e). The meridional flux of the MiS run in (Fig. 2f) displays large poleward flow in the southern mid-latitudes due to a stationary eddy over Hellas basin (Fig. 3b). This transport process is not as strong in the MuS run since less methane is transported into poleward southern latitudes by the MuS source. The zonal and meridional flux of methane for the TS run have a similar pattern to the MuS run and are displayed in Fig. 2g and h respectively. The TS simulation has a source of half the strength of the MuS run alongside an additional source over the Tharsis region with the same rate of emission (see Table 1). A stationary eddy near the additional source over the Tharsis region (Fig. 3b) increases the poleward flux of methane in the northern hemisphere and is of similar strength to the transient eddy transport (Fig. 2h). This stationary eddy also helps to provide the increased zonal flux peak of $\sim 100 \text{ kg s}^{-1}$ at 30°N in Fig. 2g, when compared to the MuS run (Fig. 2c). The methane emitted from the source over the Tharsis region is transported north by the stationary eddy and then eastward over Tempe Terra.

4.2. $L_S = 164$ – 181° : Pure advection

The atmospheric conditions for this time period are similar to the previous 30 sol period, but the peak zonal wind in each hemisphere are now at parity as the subsolar point drifts closer to the equator. The northern atmospheric jet has an increased zonal peak from 50 m s^{-1} in the previous 30 sol period to 90 m s^{-1} to now match the strength of the southern jet.

Since there is no emission from methane sources in any of the simulations, the zonal flux for all simulations is dominated by the mean zonal circulation. The main differences in Fig. 4g occur in where the peak zonal flux occur in latitude. For the MuS and TS runs, the peak zonal flux is now in northern mid-latitudes since a larger mass of methane exists in the northern hemisphere. As also noted in the previous 30 sols, the zonal and meridional flux of methane for the MuS and TS runs are very similar. The decreased mass of methane in the control run, since no methane is added to the atmosphere in the previous 30 sols, results in zonal flux peaks 5

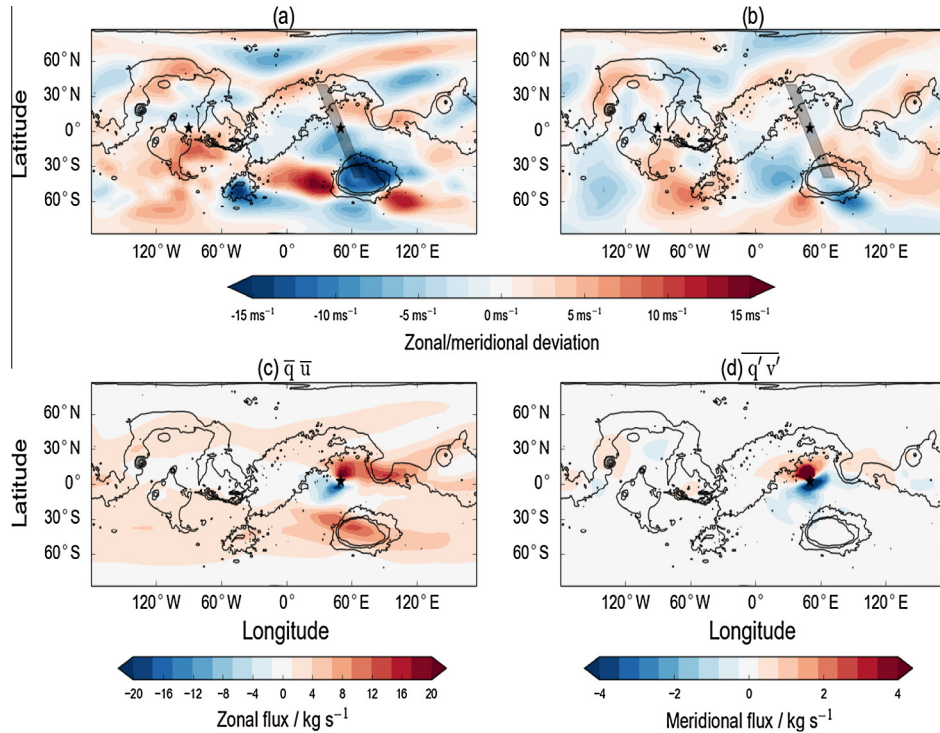


Fig. 3. Longitude–latitude plots of time-average (a) zonal and (b) meridional wind deviation from the zonal mean (for all simulations), (c) the mean zonal circulation and (d) meridional eddy transport of the MuS simulation for the time period $L_S = 148$ – 164° MY 26. Black contour lines indicate topography. The source location for the MuS and TS simulations are represented by black stars and by a shaded parallelogram for the MiS simulation in (a) and (b). The wind deviation is calculated from the surface up to 20 km since the majority of methane is located here.

times weaker in strength when compared to the other three simulations. Since the MiS run included source emission in the last 30 sol period in the southern hemisphere (as well as in the northern hemisphere), the peak zonal flux of methane is still in the southern mid-latitudes, with Fig. 4 mirror-image of Fig. 4c and g in latitude.

A stationary wave is evident at 30°N with wavenumber 2, caused by the topographical profile at this latitude (Fig. 5a). This stationary wave accounts for $\sim 10\%$ of the zonal transport at this latitude. A combination of the mean circulation in the MuS run (Fig. 5a) and the stationary wave in the 30°N latitude band creates a build up of methane over three locations: north of the Tharsis region, northwest of Nili Fossae and over Elysium Mons. This particular activity is evident in the TS run also and to a lesser extent in the MiS run, with the increased zonal flux over Hellas basin stronger than the three regions of increased activity noted above due to higher levels of methane in the southern hemisphere when compared to the MuS and TS runs.

Meridional transport of methane by stationary and transient eddies in the MuS run is still marginally more effective than the mean circulation at lower latitudes in the southern hemisphere and throughout the northern hemisphere. Peak meridional transport is around half as strong as in the previous 30 sols for all simulations. Peak poleward transport has shifted to higher latitudes of both hemispheres away from the equator. The MuS run has peak poleward transport by stationary eddies just south of the equator. This is due to increased southward transport by stationary eddies located over Nili Fossae, the Tharsis region and south of Elysium Mons (Fig. 5b). The increased mass of methane in the southern hemisphere in the MiS run provides an overall equatorward meridional flux at $\sim 45^\circ\text{S}$. This is predominantly due to transport by the mean meridional circulation ($\sim 65\%$) with increased transport equatorward on the north flank of the Argyre and Hellas basin in the MiS run (Fig. 5d). This transport process is weaker in the MuS and TS run due to lower levels of methane in these local regions.

5. Discussion

In this section, the spatial distribution of methane from the simulations is studied to identify which simulation provides transport of methane most consistent with an inferred signal by Fonti and Marzo (2010). Surface adsorption (Meslin et al., 2011) added to the best fit simulation is then explored followed by speculation on a new method of methane removal from the atmosphere. Evidence for the potential role of atmospheric dust in the temporary removal of methane is then discussed along with the relevance of this study regarding the latest measurements from the NASA Curiosity rover.

5.1. Comparing simulated methane column to the inferred signal

The column-average methane mixing ratio at $L_S = 180^\circ$ for the MuS, MiS and TS run are displayed in Fig. 6a–c respectively. At this time, a comparison to the FM10 signal (Fig. 6d) can be made. The FM10 signal is restricted to between $\pm 60^\circ$ latitude gridded into 10° latitude by 10° longitude cells and show 3 distinct peaks: over Arabia Terra, Elysium Mons and the Tharsis Montes region. For ease of comparison, the model grid is interpolated on to the same 10° latitude by 10° longitude grid as the FM10 signal.

Running the control simulation until $L_S = 180^\circ$ (not shown) provides a predominantly uniformly mixed atmosphere consistent with previous studies (Lefèvre and Forget, 2009). The difference between the maximum and minimum column-average methane mixing ratio is around 5 ppb. The inclusion of a surface source in the MuS run provides a vast improvement in the reconstruction (Fig. 6a). The evolved distribution has a maximum methane column located over Tharsis Montes consistent with the FM10 signal with no added constraint other than the strength of the source. The general spatial distribution in the MuS simulation has a strong correlation with the FM10 signal ($r(369) = 0.49$, $p < 0.01$). The peaks in

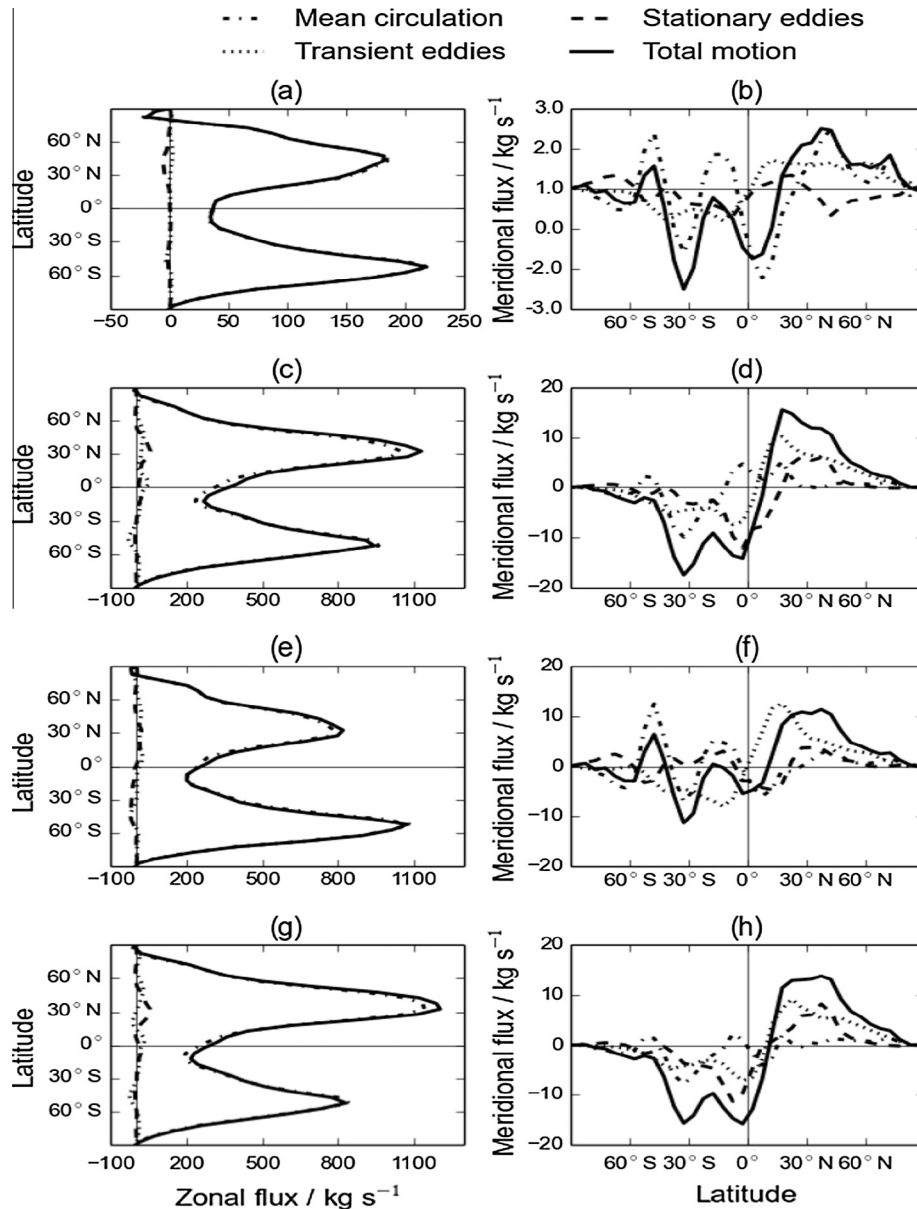


Fig. 4. Vertically integrated zonal (left) and meridional (right) flux of methane for each latitude band in the control (a and b), MuS (c and d), MiS (e and f) and TS (g and h) runs from $L_5 = 164\text{--}181^\circ$ MY 26. Note the change of scale for zonal and meridional flux in (a) and (b). Eastward and northward flux are positive.

column-average methane mixing ratio over the Tharsis Montes, Arabia Terra and Elysium Mons regions are in line with the FM10 signal with a very strong correlation ($r(52) = 0.77$, $p < 0.01$). There is an extra peak south of the Isidis basin which is difficult to reconcile due to the predominantly zonal advection of methane. To remove this peak would require a strong localised sink of methane acting frequently over this location, otherwise methane transported by westerly winds would quickly replenish the local methane abundance. These results suggest the peaks in the FM10 signal need not have come from three localised source regions, as suggested by [Fonti and Marzo \(2010\)](#), and could in fact have emanated from the single emission 60 sols earlier suggested by [Mumma et al. \(2009\)](#).

The MiS run, displayed in [Fig. 6b](#) is less consistent with the FM10 signal. The peak over the Tharsis Montes region is well matched, but the peaks over Arabia Terra and Elysium Mons are too far south. The broad source creates a higher abundance of methane in the poleward southern latitudes, whereas the FM10

signal hint at decreasing values. The source suggested by [Mischna et al. \(2011\)](#) was however an instantaneous ‘pulse’ and therefore no further continuation of this broad release is suggested. As the MuS source is located within the best fit creation of the plume identified by [Mischna et al. \(2011\)](#), they are consistent only if further emission (after the plume has initially been created) is concentrated over the location of the MuS source.

The value of Φ_m could potentially be reduced if there had been increased initial methane levels over the Tharsis Montes region (which were unobserved). This hypothesis has been tested by the TS run, with similar success to the MuS run. The TS run however has a more uniform level of methane across the peaks ([Fig. 6c](#)), with the maximum methane abundance over Tharsis at a similar level to the peaks over Arabia Terra and Elysium Mons. Slightly elevated levels over Nili Fossae in the TS run, when compared to the MuS run, indicate the methane emitted by the surface source over the Tharsis region has predominantly been transported zonally as far eastward as Nili Fossae over the 60 sol time period. With

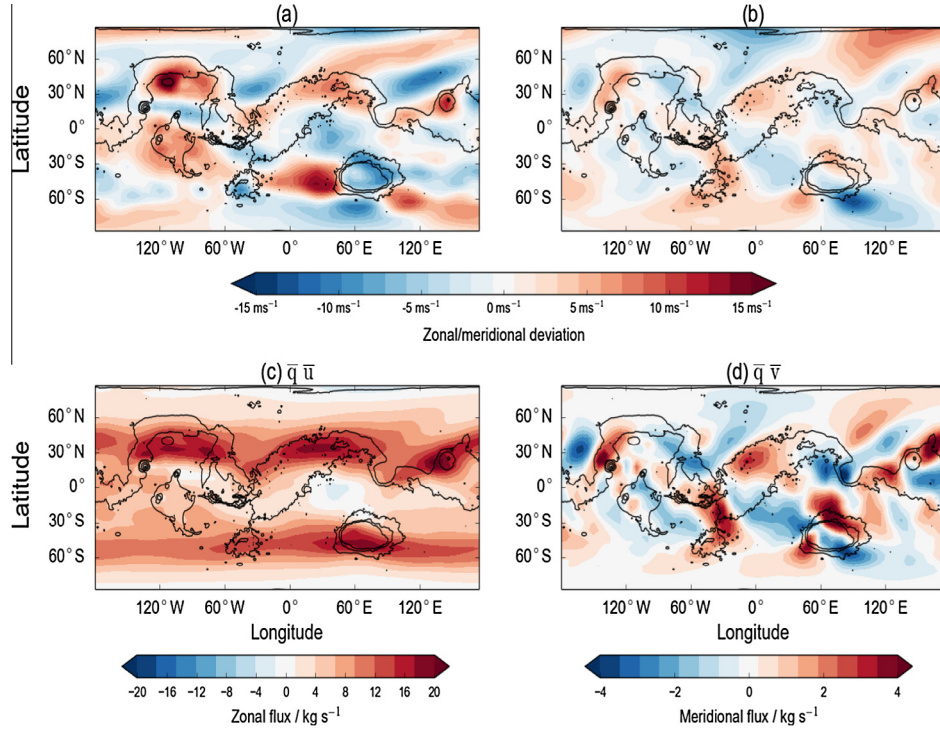


Fig. 5. Longitude–latitude plots of time-average (a) zonal and (b) meridional wind deviation from the zonal mean (for all simulations), (c) mean zonal circulation for the MuS simulation and (d) mean meridional circulation for the MiS simulation for the time period $L_S = 164$ – 181° MY 26. Black contour lines indicate topography. The wind deviation is calculated from the surface up to 20 km since the majority of methane is located here.

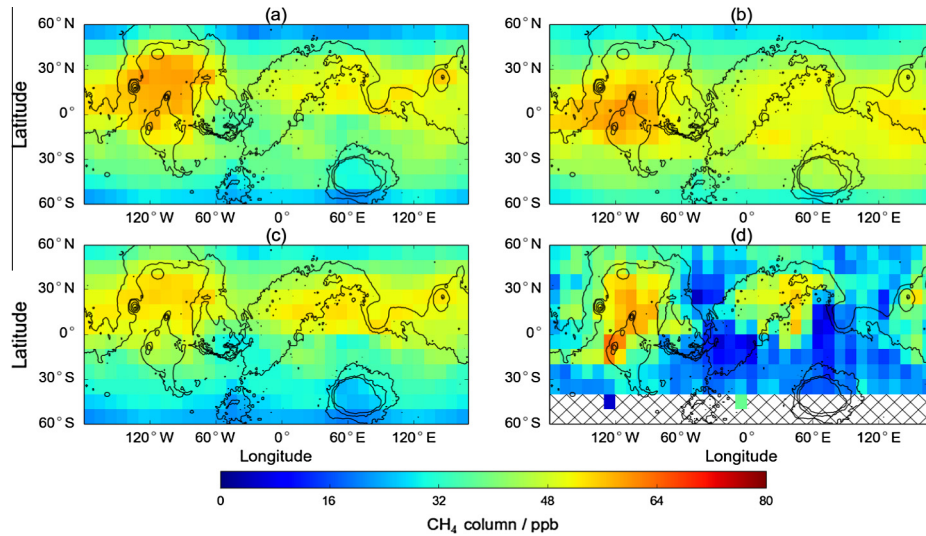


Fig. 6. Interpolated longitude–latitude plots of the column-average methane mixing ratio for the (a) MuS, (b) MiS and (c) TS simulation at $L_S = 180^\circ$. The corresponding inferred methane signal from Fonti and Marzo (2010) is displayed in (d). Black contour lines indicate topography and the hatching in (d) indicates no data is available for this location.

methane levels higher over the Tharsis region in the FM10 signal, this is suggestive of a solitary source over Nili Fossae being sufficient for the reconstruction.

5.2. Inclusion of surface adsorption

Since there are still regions in the reconstruction which necessitate a destruction mechanism to reduce the local methane level (west of Isidis basin for instance) a further simulation is run which includes a proposed sink of methane. In this model (hereafter

MuSA), the same setup as the MuS run is used but adsorption of methane on to the martian regolith with an adsorption rate consistent with previous investigations (Gough et al., 2010; Meslin et al., 2011) is also introduced. Methane surficial removal is parameterised in the MuSA model by $k_a = (\gamma \rho_b S \bar{v})/4$ where k_a is the adsorption rate (s^{-1}), γ the uptake coefficient, ρ_b the soil bulk density ($kg\ m^{-3}$), S the specific surface area ($m^2\ kg^{-1}$) and \bar{v} the mean thermal speed of CH_4 molecules ($m\ s^{-1}$) which is dependent on temperature. Values for the soil bulk density and specific surface area are $1300\ kg\ m^{-3}$ and $10^5\ m^2\ kg^{-1}$ respectively. This

mechanism is allowed to only affect the lowest layer of the atmosphere, and therefore simulate a surface sink of methane. It is an irreversible adsorption and therefore less comprehensive than the regolith diffusion model of Meslin et al. (2011). However, this is considered to be sufficient for this study where emphasis is on the net loss of methane from the atmosphere.

The uptake coefficient has been derived from laboratory experiments on the JSC-1 Mars martian soil analogue (Gough et al., 2010) and is temperature dependent, following $\gamma = \exp((-45.41 + |\Delta H_{obs}|)/RT)$ where ΔH_{obs} is a lower limit of the enthalpy of adsorption (kJ mol^{-1}), T is the temperature and R is the ideal gas constant ($8.314 \text{ J K}^{-1} \text{ mol}^{-1}$). ΔH_{obs} was experimentally determined by Gough et al. (2010) to have a value of $-18.08 \text{ kJ mol}^{-1}$. The temperature dependence of the adsorption rate results in increased adsorption at lower temperatures, with a drop in the adsorption rate of two orders of magnitude from 150 to 280 K (Fig. 7a).

The adsorption occurs most strongly around the south pole, extending up to 45°S latitude, where surface temperatures are at their lowest at around 140–145 K ($L_S = 155\text{--}180^\circ$ corresponds to the end of southern winter). In the poleward northern latitudes, adsorption only begins to have a noticeable effect after 30 sols. Surficial adsorption of methane also occurs in the mid-latitudes at high altitudes (such as around Olympus Mons) and due to the diurnal variability of surface temperatures which can reach as low as 150 K at Solis Planitia at nighttime.

The methane column at $L_S = 180^\circ$ of the MuSA model is shown in Fig. 7b and can be compared to the FM10 signal (Fig. 6d). The pockets of lower methane abundance north of both the Argye and Hellas basins in the FM10 signal are difficult to reconcile even using the MuSA model, suggesting even more localised destruction.

The failure to reach the minimum levels, particularly considering there is no desorption in this model, implies the adsorption is too slow as indicated by Meslin et al. (2011). The correlation between the MuSA simulation and the FM10 signal decreases ($r(369) = 0.47$, $p < 0.01$) when compared to the MuS simulation. Trainer et al. (2010) concluded that trapping of methane in the polar ice caps is practically negligible which also limits this method of adsorption, since it occurs primarily over the polar regions. The mechanism of surface adsorption for the destruction of methane is evidently not a viable option.

5.3. Methane removal by zeolite in martian dust?

A potential methane sink which has been overlooked so far is the possible presence of zeolite in atmospheric dust particles. Methane reacts weakly with most surfaces, but some zeolites have recently been suggested as a material that can trap methane (Kim

et al., 2013). Spectral evidence from the dusty martian surface (Ruff, 2004) along with CRISM measurements west of Nili Fossae (Ehlmann et al., 2009) point to the possibility of zeolites being a component of the martian surface and potentially the atmosphere. Meslin et al. (2011) note that the adsorption rate for zeolites is larger than the standard martian regolith and the proposed mechanism here would be capable of removing methane from higher altitudes than just the surface dust. Airborne dust also has an advantage in potentially creating the spatial variations seen in observations since a dust particle at higher altitude would be capable of quickly carrying the adsorbed methane away from the site of adsorption.

Dust devils, which have been observed numerous times (Thomas and Gierasch, 1985; Edgett and Malin, 2000; Greeley et al., 2006), could also provide local-scale variations of methane, and potentially induce at least partially the temporal and spatial methane variations seen in the observations. The JSC-1 Mars analog contains no signature of zeolites and so any additional uptake due to the presence of this substance is not present in the measured coefficient. Regarding the additional peak in the modelled distribution on the south flank of the Isidis basin (see Fig. 6a), flushing dust storms have been shown to start at the Isidis planitia in model simulations (Mulholland et al., 2013). Although these primarily occur at $L_S = 210^\circ$, which is a short time after the FM10 signal, trapping of methane in these flushing dust storms could be seen as a possible mechanism that could provide the fast removal of methane in this localised region.

Full understanding of the spatial variability of zeolites is also currently lacking. The zeolite proposed here would have to be a specific designer material which preferentially adsorbs methane over other atmospheric constituents such as CO_2 . Kim et al. (2013) find only a couple of hypothetical zeolite structures which could perform this task, and so the temporary removal mechanism described here is currently not conclusive. Information on the rates of trapping/release of methane by this proposed storage mechanism are currently unknown and would require further study. Frequent observations of the methane distribution, with greater certainty, would provide a more stringent comparison to determine if this destruction mechanism is a viable option. Future orbiter missions such as the ExoMars Trace Gas Orbiter (TGO), scheduled for launch in 2016, will provide global methane retrievals with good temporal and spatial coverage.

5.4. Recent observations by the Curiosity rover

Potential evidence for atmospheric dust playing a role in the removal of methane is seen in the latest measurements by the NASA Curiosity rover (Webster et al., 2015). They have indicated a possible anti-correlation between methane and atmospheric

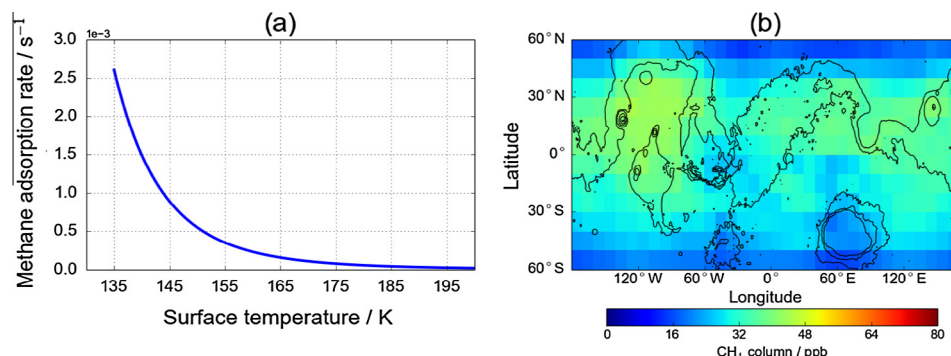


Fig. 7. (a) Surface temperature plotted against the methane adsorption rate for the MuSA simulation. The formula for methane adsorption is the same as in (Meslin et al., 2011). (b) Interpolated longitude–latitude plot of the column-average methane mixing ratio for the MuSA simulation at $L_S = 180^\circ$. Black contour lines indicate topography.

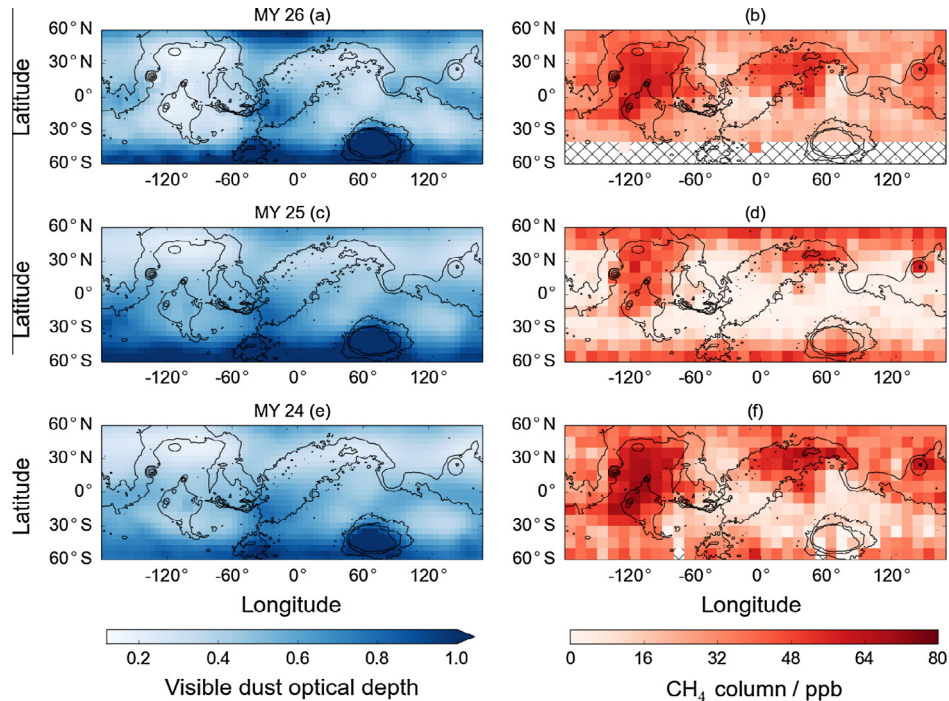


Fig. 8. Average visible dust optical depth (left) from the simulations for the 30 sol period leading up to the FM10 signal (right). Mars year is in reverse order from MY 26 (top row) to MY 24 (bottom row).

opacity, suggestive that atmospheric dust could possibly be involved in the process of removing methane from the atmosphere. To test this hypothesis with the FM10 signal, the 30 sol average dust optical depth leading up to $L_s = 180^\circ$ is compared to the FM10 signal for three Mars years (Fig. 8). There is a strong anti-correlation coefficient of $r(369) = -0.51$ ($p < 0.01$) for MY 26 and $r(428) = -0.40$ ($p < 0.01$) for MY 24, with no correlation evident for MY 25. The area north of Argyre basin, which is still outstanding in all simulations, shows increased dust levels compared to the ambient atmospheric dust opacity. An atmospheric sink related to the dust opacity would therefore lower the levels over this region, more in line with the FM10 signal.

Lower levels of dust are present in the poleward northern and mid latitudes, meaning these regions would be relatively unaffected if a currently unknown sink involving atmospheric dust is present. The FM10 signal for multiple Mars years indicate the lowest levels of methane in the atmosphere occur around $L_s = 270^\circ$, just after peak dust activity (Fonti and Marzo, 2010). Caution must be taken with this analysis however due to the relatively large FM10 signal uncertainty of $\sim \pm 25\%$ for MY 24/26 and $\sim \pm 40\%$ for MY 25.

Following an initial upper limit of 1.3 ppb in Gale crater measured by the NASA Curiosity rover at around $L_s = 180^\circ$ in MY 31 (Webster et al., 2013), more recent measurements have observed a sudden increase to around 7 ppb (Webster et al., 2015) for a short 60 sol period. A case is made by Webster et al. (2015) that these measurements best fit a local source which terminates quickly. The latest measurements could potentially be consistent with source emission and previous higher methane retrievals under certain conditions. Firstly, the plume observed by Mumma et al. (2009) must not be an annual event, which is entirely plausible. Secondly, the release of additional methane into the atmosphere by surface emission or by other means must be fairly limited leading up to the Curiosity rover measurement by Webster et al. (2015). A GCM can be used to investigate whether surface source emission could account for the observed increase in this local

region, how strong it would need to be and where it is likely to be spatially located.

Whether the conditions described above are credible is difficult to know due to the lack of regular published global methane observations from the end of MY 26 to the present time. If a methane sink is apparent on Mars, the lower levels of the Curiosity rover measurements when compared to previous results (Mumma et al., 2009; Fonti and Marzo, 2010) can be explained by a relative lack of, or indeed complete absence of, methane source emission in the intervening period. The ExoMars TGO will provide regular methane observations in the future. The distribution of any spatial variations seen by the ExoMars TGO can be studied by a GCM, in a similar manner to this investigation, with the aim of identifying how the spatial variations are formed.

6. Conclusions

During this investigation a GCM model is used as a tool to determine whether different observations of methane can be mutually consistent. Although the passive model showed little similarity to the observations, a simulation including additional source emission is shown to improve the match between previous observations. A potential source over the Tharsis region is plausible but less consistent with both sets of observations than a solitary source over Nili Fossae. An additional peak on the south flank of the Isidis basin is not observed in the FM10 signal, but hard to remove from the model due to the dominant zonal transport.

Including a surficial adsorption parameterisation alone did not improve the reconstruction. A combination of both continued source emission and adsorption however cannot be ruled out. A zeolite structure present in dust storms is suggested here as a new potential mechanism to trap methane, potentially bringing the modelled behaviour of emitted methane into line with observations. Availability of adsorption sites on the dust particles would provide an effective mechanism to destroy methane throughout most of the lower atmosphere.

The strength of methane release and uptake is an issue which remains unresolved. The synthesis of observations is improved when the source over Nili Fossae continues to emit after the observations have been made, but for less than the whole 60 sol period leading up to the FM10 signal. The efficiency of atmospheric mixing means constraints on the timescale and cessation of emissions are key to accurately identifying the strength of methane release.

By investigating the transport diagnostics of methane, it is proposed that the three localised sources identified by [Fonti and Marzo \(2010\)](#) for northern autumn MY 26 could in fact be a result of the evolution of the methane plume observed earlier in the year by [Mumma et al. \(2009\)](#). It is difficult to verify decisively the simulation results without regular observations in the time window, especially regarding the latest measurement by the Curiosity rover. A GCM can be used to investigate whether surface source emission could account for the observed increase in Gale crater. The ExoMars TGO, due for launch in 2016, will provide an ideal dataset to analyse the validity of past observations and, in conjunction with a GCM, explore the global distribution of martian methane.

Acknowledgments

The authors thank two anonymous referees for their constructive comments which have resulted in a substantial improvement to the paper. JAH and SRL thank the UK Space Agency for support under Grant ST/I003096/1, SRL thanks STFC for support under Grant ST/J001597/1 and MRP thanks the UK Space Agency for support under Grant ST/I003061/1. Thanks also to Sergio Fonti and Giuseppe Marzo for access to the TES methane retrievals. We are grateful for an ongoing collaboration with François Forget and coworkers at LMD and Franck Lefèvre at LATMOS. Model results are available from the authors upon request. This work is funded under the UKSA Aurora programme.

References

- Atreya, S.K. et al., 2006. Oxidant enhancement in martian dust devils and storms: Implications for life and habitability. *Astrobiology* 6, 439–450.
- Atreya, S.K., Mahaffy, P.R., Wong, A.-S., 2007. Methane and related trace species on Mars: Origin, loss, implications for life, and habitability. *Planet. Space Sci.* 55, 358–369.
- Edgett, K.S., Malin, M.C., 2000. Martian dust raising and surface albedo controls: Thin, dark (and sometimes bright) streaks and dust devils in MGS MOC high resolution images. In: Lunar and Planetary Institute Science Conference Abstracts, Lunar and Planetary Inst. Technical Report, vol. 31, p. 1073.
- Ehlmann, B.L. et al., 2009. Identification of hydrated silicate minerals on Mars using MRO-CRISM: Geologic context near Nili Fossae and implications for aqueous alteration. *J. Geophys. Res. (Planets)* 114, E00D08.
- Farrell, W.M., Delory, G.T., Atreya, S.K., 2006. Martian dust storms as a possible sink of atmospheric methane. *Geophys. Res. Lett.* 33, L21203.
- Fonti, S., Marzo, G.A., 2010. Mapping the methane on Mars. *Astron. Astrophys.* 512, A51.
- Forget, F. et al., 1999. Improved general circulation models of the martian atmosphere from the surface to above 80 km. *J. Geophys. Res.* 104, 24155–24176.
- Formisano, V. et al., 2004. Detection of methane in the atmosphere of Mars. *Science* 306, 1758–1761.
- Gough, R.V. et al., 2010. Methane adsorption on a martian soil analog: An abiogenic explanation for methane variability in the martian atmosphere. *Icarus* 207, 165–174.
- Gough, R.V. et al., 2011. Can rapid loss and high variability of martian methane be explained by surface H₂O₂? *Planet. Space Sci.* 59, 238–246.
- Greeley, R. et al., 2006. Active dust devils in Gusev crater, Mars: Observations from the Mars Exploration Rover Spirit. *J. Geophys. Res. (Planets)* 111, E12S09.
- Hinson, D.P., 2006. Radio occultation measurements of transient eddies in the northern hemisphere of Mars. *J. Geophys. Res. (Planets)* 111, E05002.
- Kim, J. et al., 2013. New materials for methane capture from dilute and medium-concentration sources. *Nature Comms.* 4, 1694.
- Krasnopolsky, V.A. et al., 2004. Detection of methane in the martian atmosphere: Evidence for life? *Icarus* 172, 537–547.
- Lefèvre, F., Forget, F., 2009. Observed variations of methane on Mars unexplained by known atmospheric chemistry and physics. *Nature* 460, 720–723.
- Lewis, S.R. et al., 2007. Assimilation of Thermal Emission Spectrometer atmospheric data during the Mars Global Surveyor aerobraking period. *Icarus* 192, 327–347.
- Meslin, P.-Y. et al., 2011. Little variability of methane on Mars induced by adsorption in the regolith. *Planet. Space Sci.* 59, 247–258.
- Mischina, M.A. et al., 2011. Atmospheric modeling of Mars methane surface releases. *Planet. Space Sci.* 59, 227–237.
- Montabone, L. et al., 2015. Eight-year climatology of dust optical depth on Mars. *Icarus* 251, 65–95.
- Mulholland, D.P., Read, P.L., Lewis, S.R., 2013. Simulating the interannual variability of major dust storms on Mars using variable lifting thresholds. *Icarus* 223, 344–358.
- Mumma, M.J. et al., 2009. Strong release of methane on Mars in northern summer 2003. *Science* 323, 1041–1045.
- Newman, C.E. et al., 2002. Modeling the martian dust cycle, 1. Representations of dust transport processes. *J. Geophys. Res.* 107, 6-1–6-18.
- Peixoto, J.P., Oort, A.H., 1992. *Physics of Climate*. American Institute of Physics.
- Priestley, A., 1993. A quasi-conservative version of the semi-lagrangian advection scheme. *Mont. Weath. Rev.* 121, 621–629.
- Ruff, S.W., 2004. Spectral evidence for zeolite in the dust on Mars. *Icarus* 168, 131–143.
- Stevens, A.H., Patel, M.R., Lewis, S.R., 2015. Numerical modelling of the transport of trace gases including methane in the subsurface of Mars. *Icarus* 250, 587–594.
- Thomas, P., Gierasch, P., 1985. Dust devils on Mars. In: Lunar and Planetary Institute Science Conference Abstracts, Lunar and Planetary Inst. Technical Report, vol. 16, p. 857.
- Trainer, M.G. et al., 2010. Limits on the trapping of atmospheric CH₄ in martian polar ice analogs. *Icarus* 208, 192–197.
- Webster, C.R. et al., 2013. Low upper limit to methane abundance on Mars. *Science* 342, 355–357.
- Webster, C.R. et al., 2015. Mars methane detection and variability at Gale crater. *Science* 347, 415–417.